Applied Catalysis B: Environmental 168-169 (2015) 550–558

Contents lists available at ScienceDirect

Applied Catalysis B: Environmental

journal homepage: www.elsevier.com/locate/apcatb

The fabrication of innovative single crystal N,F-codoped titanium dioxide nanowires with enhanced photocatalytic activity for degradation of atrazine

Yanlin Zhang[a,c,d], Changseok Han[b], Mallikarjuna N. Nadagouda[e], Dionysios D. Dionysiou[b,f,*]

[a] School of Chemistry & Environment, South China Normal University, Guangzhou 510006, China
[b] Environmental Engineering and Science Program, Department of Biomedical, Chemical and Environmental Engineering (DBCEE), University of Cincinnati, OH 45221-0012, USA
[c] Key Laboratory of Theoretical Chemistry of Environment Ministry of Education, South China Normal University, Guangzhou 510006, China
[d] Guangdong Technology Research Center for Ecological Management and Remediation of Urban Water System, School of Chemistry & Environment, South China Normal University, Guangzhou 510006, China
[e] College of Pharmacy, Sangolli Rayanna Nagar, Dharwad 580002, India
[f] Nireas-International Water Research Centre, University of Cyprus, Nicosia 20537, Cyprus

ARTICLE INFO

Article history:
Received 14 July 2014
Received in revised form 2 January 2015
Accepted 9 January 2015
Available online 12 January 2015

Keywords:
Titanium dioxide nanowires
Nonmetal codoping
Photodegradation
Photocatalysis
Atrazine

ABSTRACT

N,F-codoped TiO_2 nanowires were synthesized using titanium sulfate as a Ti precursor and isopropanol as a protective capping agent by a hydrothermal route. The obtained doped nanowires were characterized by XRD, SEM, TEM, HRTEM, SAED, XPS, porosimetry analysis and UV–vis diffuse reflectance spectroscopy. The synthesized N,F-codoped TiO_2 nanowires calcined at 500 °C have TiO_2 (B) and anatase phase and then are completely transformed to anatase phase after calcination at 600 °C. Photocatalytic activity measurements show that the N,F-codoped TiO_2 nanowires calcined at 600 °C possess the best photocatalytic performance for the degradation of atrazine under UV and visible light irradiation in comparison with N,F-codoped TiO_2 nanoparticles and N-doped TiO_2 nanowires, which was attributed to the relatively more quantity of active {0 0 1} crystal facet due to the addition of F^- and the synergistic effect of N and F doping.

1. Introduction

Since carbon nanotubes were discovered by Ajayan and Iijima in 1993 [1], nanoscale materials have attracted great interest due to their unique structure, electronic and optical properties and potential applications in photocatalysis, gas sensing, solar cells, and fuel cells. Among them, nanostructured TiO_2 is especially interesting due to its large surface area and unique interface, which makes it of higher importance application in photo-splitting of water [2], photocatalysis [3], and photovoltaics [4]. However, the wide bandgap of TiO_2 (i.e., 3.2 eV for anatase) requires UV light for its activation. A promising approach to achieve visible-light-responsive activity is doping with a non-metal element such as N, C, S or B [5–9]. Among them, N-doped TiO_2 seems to be the most efficient and extensively investigated. Compared to single non-metal dopant, doping with two different non-metal elements such as S and N atoms [10,11], C and N atoms [12–14], B and N [15,16], and F and N atoms [5] have demonstrated more appreciable effects.

Among various properties of nanoscale materials, one-dimensional (1D) structure of such materials is greatly desired as it has higher charge carrier mobility and lower carrier recombination rate [17]. The speed of electron diffusion across nanoparticle junctions is several orders of magnitude smaller than that of 1D crystalline material due to frequent electron trapping at the junctions of nanoparticles [18]. In this case, separated charges are easily recombined before they reach the surface of nanoparticles. The 1D nanostructures such as nanowires and nanotubes have been suggested to eliminate such drawbacks [19,20]. Nanowires and nanotubes can provide a pathway of transporting charges without grain boundaries and junctions. Once electrons are injected to the conduction band of TiO_2, the recombination of electron and holes can be minimized due to their relatively wide bandgap [21].

* Corresponding author at: Environmental Engineering and Science Program, Department of Biomedical, Chemical and Environmental Engineering (DBCEE), University of Cincinnati, OH 45221-0012, USA. Tel.: +1 5135560724; fax.: +1 5135564162.

http://dx.doi.org/10.1016/j.apcatb.2015.01.009
0926-3373/

Another advantage of 1D nanostructures is the ability to capture scattered light in the cell, which is possible to increase light harvesting [21]. In addition, 1D TiO_2 materials still have the characteristics of high surface area and nanosize effect because they are nanosized in their diameter [22]. These 1D TiO_2 materials are also allowed to be more easily separated and recovered than TiO_2 nanoparticles due to the length of 1D TiO_2 materials in a micrometer range.

Although the nanotube structure is attractive due to its high specific surface area, TiO_2 and titanate nanotubes are usually unstable at high temperatures (>500 °C) since their nanotube structure can convert into particles [23,24]. Therefore, the nanowires are typically more favorable to maintain the 1D nanostructure at high temperature from 500–800 °C.

Different strategies have been developed for synthesizing TiO_2 nanowires (TiO_2 NWs) including reactive sputtering [25], hydrolysis [26], chemical vapor deposition [27], and thermal treatment [28]. Among the synthesis strategies of TiO_2 NWs so far, a hydrothermal method is one of the most promising and widely used methods because the process dramatically decreases the required temperature for the growth of nanowires from 850 °C to 180 °C [3,29] through the use of acetone as the oxygen source for Ti oxidation. Moreover, a more alkaline environment reduces the required processing temperature. The reaction temperature decreased from 230 to 180 °C when the concentration of NaOH increased from 1 to 10 M for the growth of titanate nanowires [30,31].

Although much effort has been made on the preparation of pure TiO_2 NWs [32], much less work is done on non-metal-codoped TiO_2 NWs. This is because anatase nanowires usually have very high crystallinity, making it hard to incorporate dopants into their lattice by mild post-heat-treatment. In most of chemical doping routes, TiO_2 was treated at higher temperature up to 400 °C in the presence of NH_3 or N_2 gas, which is not a facile way [33]. Also, the addition of dopant precursors in a reaction medium can often negatively influence the nucleation and growth of anatase TiO_2 NWs and lead to obtain non-desirable doped TiO_2 NWs. Thus, it is of great significance to develop a facile method to synthesize the non-mental-codoped TiO_2 NWs.

In this paper, N,F-codoped TiO_2 NWs (NF–TiO_2 NWs) were synthesized by a hydrothermal treatment using titanium sulfate powders as a Ti source. We found that ammonium fluoride doping in the process of hydrothermal synthesis can decrease the surface energy of {0 0 1} crystal facet and correspondingly increase the amount of {0 0 1} facet, which is a more reactive facet relative to {1 0 1} facet. As a kind of triazine herbicides widely used for crops and weed control, atrazine is photolyzed slowly by sunlight and is also resistant to microorganism degradation; it is therefore persistent in water and soil. We use atrazine as a target contaminant to evaluate the photocatalytic activity of synthesized photocatalysts. NF–TiO_2 NWs demonstrated higher photocatalytic activity for degradation of atrazine than NF–TiO_2 nanoparticles under visible light and UV light illumination. Considering the facile nature of this hydrothermal method, the synthesized TiO_2 NWs in this study have a great potential in the degradation of organic pollutants, solar energy conversion, and water splitting for hydrogen generation.

2. Experimental

2.1. Synthesis of TiO_2 photocatalysts

In a typical synthesis, 1.6 g of titanium sulfate (ACS reagent, MP Biomedicals), 0.076 g of urea (ACS reagent, Fisher Scientific) and 0.092 g of ammonium fluoride (ACS reagent, MP Biomedicals) were added to the mixture of 40 mL deionized water and 30 mL isopropanol (ACS reagent, Pharmco). Then the obtained suspension was adjusted to pH 7 by addition of 1.0 M NaOH (ACS reagent, Fluka) and subsequently put into a Teflon-lined stainless autoclave

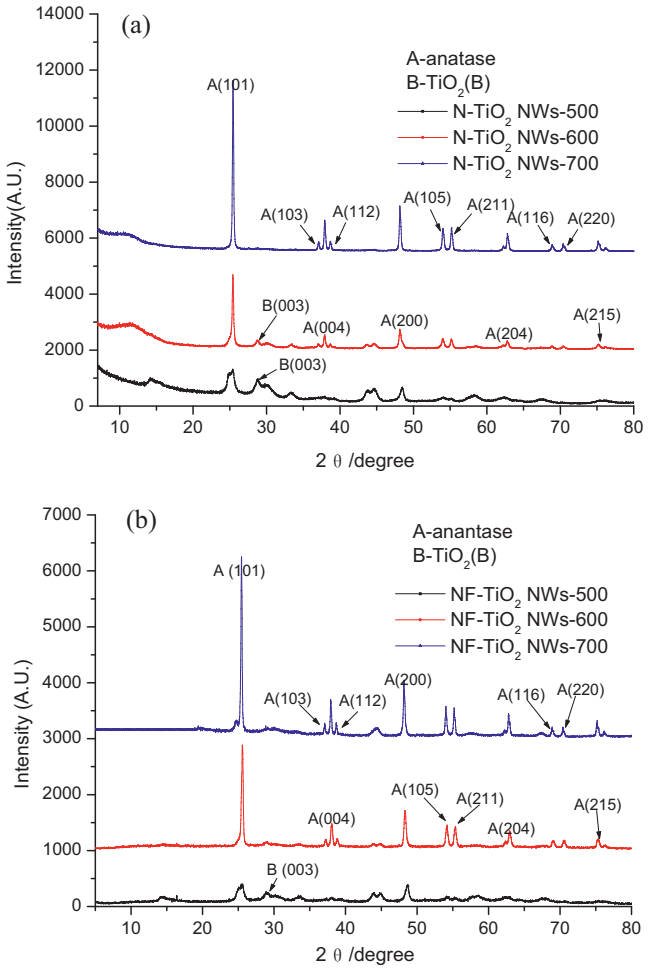

Fig. 1. XRD analysis for N–TiO_2 NWs and NF–TiO_2 NWs.

for hydrothermal treatment at 140 °C for 16 h. After that, the obtained precipitates were cooled to room temperature. Subsequently, 60 mL of 10.0 M NaOH was added to the above cooled precipitates and continued to hydrothermally treat in the same autoclave at 200 °C for 48 h. The final obtained precipitates were then washed by deionized water, centrifuged, and transferred to 500 mL of 0.1 M HCl aqueous solution and kept constantly stirred for 12 h. After HCl treatment, the obtained precipitates were centrifuged and thoroughly washed by deionized water. The final obtained product NF–TiO_2 NWs was dried at 80 °C for 24 h. TiO_2 NWs and N–TiO_2 NWs were synthesized by the same method as preparing NF–TiO_2 NWs without the addition of ammonium fluoride and/or urea at the beginning. All prepared nanowires were calcined in air atmosphere at 500–700 °C for 2 h in order to study the effect of post-heat treatment on their crystal structure. The preparation method of NF–TiO_2 nanoparticles (NPs) is as follows: 1.6 g of titanium sulfate, 0.076 g of urea and 0.092 g of ammonium fluoride were added to 40 mL distilled water and 30 mL 2-propanol. Then the obtained suspension was adjusted to pH 12 by addition of 1.0 M NaOH and subsequently put into a Teflon-lined stainless autoclave to hydrothermally treat at 140 °C for 16 h. The synthesized product was dried at 80 °C for 24 h and calcined in air atmosphere at 600 °C for 2 h.

2.2. Characterization of TiO_2 NWs

The crystal structures of synthesized doped TiO_2 NWs were determined using a Bruker D8 Advance XRD diffractometer (Bruker). A Tristar 3000 (Micromeritics) porosimeter analyzer was

used to determine Brunauer, Emmett, and Teller (BET) surface area, pore volume, Barrett–Joyner–Halenda (BJH) pore size and pore size distribution after the samples were purged with nitrogen gas for 2 h at 150 °C using Flow prep 060 (Micromeritics). The photocatalyst morphology was characterized by an environmental scanning electron microscope (ESEM, Philips XL 30 ESEM-FEG). Optoelectronic properties were derived from diffuse reflectance spectra obtained on a UV–vis spectrophotometer (Shimadzu 2501PC) equipped with an integrated sphere attachment (ISR 1200). $BaSO_4$ was a reference standard material. To determine the fine elemental composition and electronic structure, X-ray photoelectron spectroscopy (Axis Ultra DLD, Kratos) with Mono AlKα X-rays at vacuum pressure of $\sim 5 \times 10^{-9}$ Torr was employed. The binding energies were corrected based on C1s level peak at 284.6 eV. A JEM-2010F (JEOL) high-resolution transmission electron microscope (HRTEM) with field emission gun at 200 kV was used to obtain information on crystal size and crystal structure. The samples were prepared in isopropanol (HPLC grade, Pharmco) using an ultrasonicator (2510R-DH, Bransonic) over 30 min and then fixed on a carbon coated copper grid (FCF400-Cu, FROMVAR).

2.3. Photocatalytic activity

A borosilicate glass petri dish (dia.6 cm) was used to evaluate the photocatalytic activity of synthesized doped TiO_2 NWs. The total volume of the solution was 10 mL and the initial concentration of atrazine was 5 mg L^{-1} in the glass petri dish. Then 0.01 g of TiO_2 NWs was placed in the solution to form the photocatalyst suspension. For all experiments, MilliQ grade water was used. This suspension was magnetically stirred in the dark for 30 min before light irradiation to ensure the establishment of an adsorption/desorption equilibrium of atrazine on the surface of photocatalysts.

For visible light irradiation, two 15 W fluorescent lamps (intensity: 3.99×10^{-4} W cm^{-2} [34], Philips) were used as a visible light source, a UV block filter (UV420, Opticology) was mounted under the light source. For UV light irradiation, two 15 W UV light lamps (365 nm wavelength, intensity 2.47×10^{-3} W cm^{-2}, Philips) were used. A 0.2 mL sample was withdrawn at different time. The concentration of atrazine in the samples was quantified using a high-performance liquid chromatograph (HPLC, Agilent Series 1100) under the detectable wavelength of 220 nm for atrazine. An Agilent Eclipse C8 column (150 mm × 4.6 mm, particle size 5 μm) was employed. The elution phase is the mixture of 40% SQ water (ultra-pure water, Fluka Co.) and 60% acetonitrile. The flow rate was 0.4 mL min^{-1} and the injection volume was 20 μL. The retention time of atrazine was 6.7 min.

3. Results and discussion

The crystal structure of N–TiO_2 NWs and NF–TiO_2 NWs after calcination at different temperatures was determined by XRD. The results shown in Fig. 1 indicated that both N–TiO_2 NWs and NF–TiO_2 NWs at the calcination of 500 °C were a mixture of TiO_2 (B) and anatase phase. TiO_2 (B) is a metastable polymorph that usually forms by dehydration of a layered structured hydrogen titanate. After calcination at 600 °C for N–TiO_2 NWs (Fig. 1(a)), the TiO_2 (B) phase was partially transformed into anatase TiO_2. These XRD patterns were in good agreement with the previously reported results [35]. For NF–TiO_2 NWs, the TiO_2 (B) phase were completely transformed to anatase after calcination at 600 °C. After calcination at 700 °C, two doped nanowires were composed of anatase phase only without rutile phase. This result indicated that the initial formation of the TiO_2 (B) phase indeed could inhibit the transformation of anatase to rutile at higher calcination temperature (i.e., 700 °C) [36].

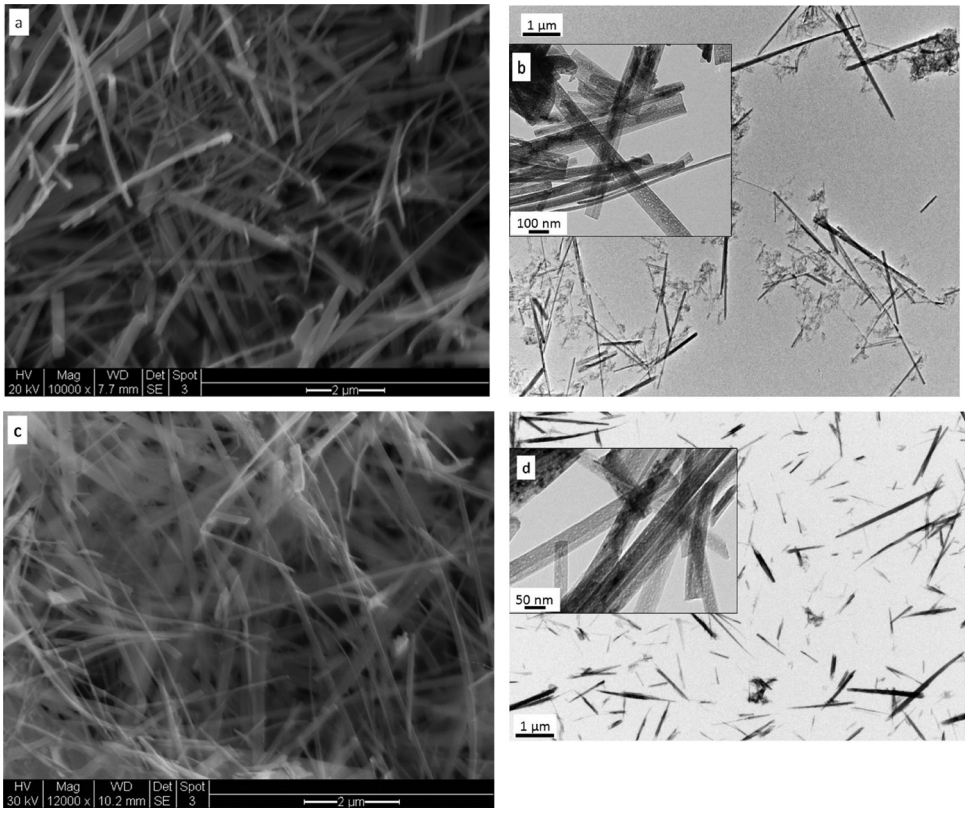

Fig. 2. SEM images of (a) N–TiO_2 NWs, (c) NF–TiO_2 NWs, and TEM images of (b) N–TiO_2 NWs, (d) NF–TiO_2 NWs. (inset TEM images are magnification ones).

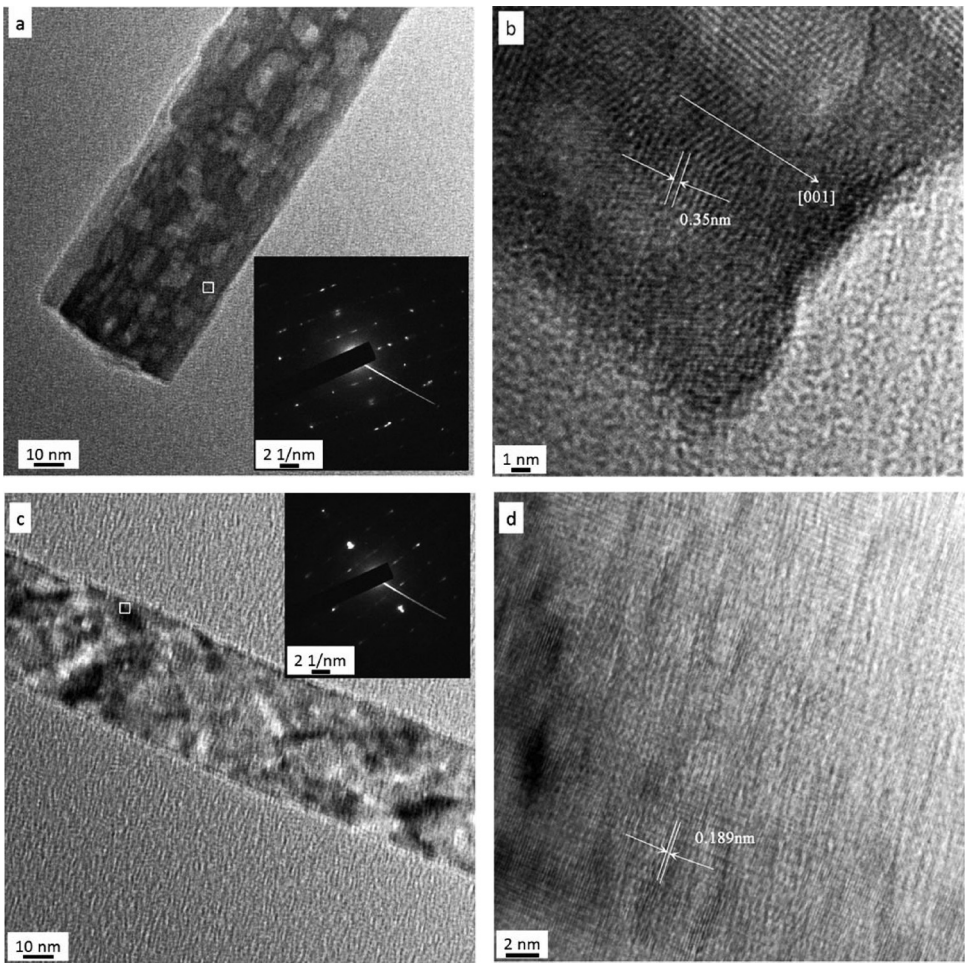

Fig. 3. (a) TEM (inset for SAED pattern) image, (b) HRTEM image of N–TiO_2 NWs calcined at 600 °C, and (c) TEM (inset for SAED pattern) image, (d) HRTEM image of NF–TiO_2 NWs calcined at 600 °C.

Figs. 2 and 3 show the representative SEM and HRTEM images of N–TiO_2 NWs and NF–TiO_2 NWs. These two nanowires with an average diameter of ~50–100 nm and an average length of ~1–5 μm were observed from the SEM and TEM images (Fig. 2a–d) of doped TiO_2 NWs. HRTEM (Fig. 3b and d) and SAED (3a inset and 3c inset) images further confirm the single-crystalline characteristics of N–TiO_2 NWs and NF–TiO_2 NWs. The HRTEM image of N–TiO_2 NWs (Fig. 3b) shows the {1 0 1} planes of TiO_2 anatase phase with lattice spacing of 0.35 nm. Moreover, the axis of the nanowire was parallel to the [001] direction, indicating that the nanowire grows along the [001] direction. The angle between [101] and [001] directions is 63°, which was in good agreement with the model of single crystal anatase TiO_2. Therefore, it can be concluded that the single crystallinity of N–TiO_2 nanowire is composed predominately by the thermodynamically stable {1 0 1} facet. It should be noted that the {0 0 1} exposing percentage is generally less than 6% according to the Wulff construction [37].

The SAED patterns in Fig. 3c inset record from the white squared area in Fig. 3c can be indexed into diffraction spots of the [001] zone. The corresponding HRTEM image in Fig. 3d shows that the {2 0 0} and {0 2 0} atomic facets with a lattice spacing of 0.189 nm and an interfacial angle of 90°. The above results demonstrate that the percentage of obtained single crystalline NF–TiO_2 NWs with exposed {0 0 1} circumferential surfaces was more than that of N–TiO_2 NWs [38,39]. This unique structure could be beneficial to the photocatalytic oxidation of contaminants.

The initial overall reactions by using Ti $(SO_4)_2$ as a precursor in the synthesis before hydrothermal growth follows:

$$Ti(SO_4)_2 + 4NaOH = H_2TiO_3 + 2Na_2SO_4 + H_2O \quad (1)$$

In the first period of NF–TiO_2 NWs hydrothermal growth (140 °C, 16 h), ammonium fluoride was first decomposed into ammonia and hydrogen fluoride under the conditions of neutral pH and heating in terms of physical and chemical properties of urea and ammonium fluoride. The decomposed ammonia could be doped into precursor titanate in the enclosed autoclave. However, urea could not be composed in the present conditions of pH and temperature. When the reaction extended into the second period, urea was heated to 200 °C in alkaline solution and decomposed into ammonia, which was doped into the titanate as the source of nitrogen. Thus the source of nitrogen comes from both urea and ammonium fluoride. The ammonium fluoride used in this work not only acts as nitrogen and fluorine source but can also create a fluorine-rich environment on the crystal surface and promote the preferred growth of the {0 0 1}facet due to the low F–F binding energy (158.8 $kJmol^{-1}$) and high F–Ti binding energy (569.0 $kJmol^{-1}$) that can significantly lower the energy of the {0 0 1} surface. First-principles calculations also indicate that fluorine ions can greatly reduce the surface energy of {0 0 1} facet, making them more stable than the {1 0 1} facet [40].

The formation of 1D nanomaterial with high reactive crystal facets depends on R_F (nominal molar ratios of fluorine to titanium)

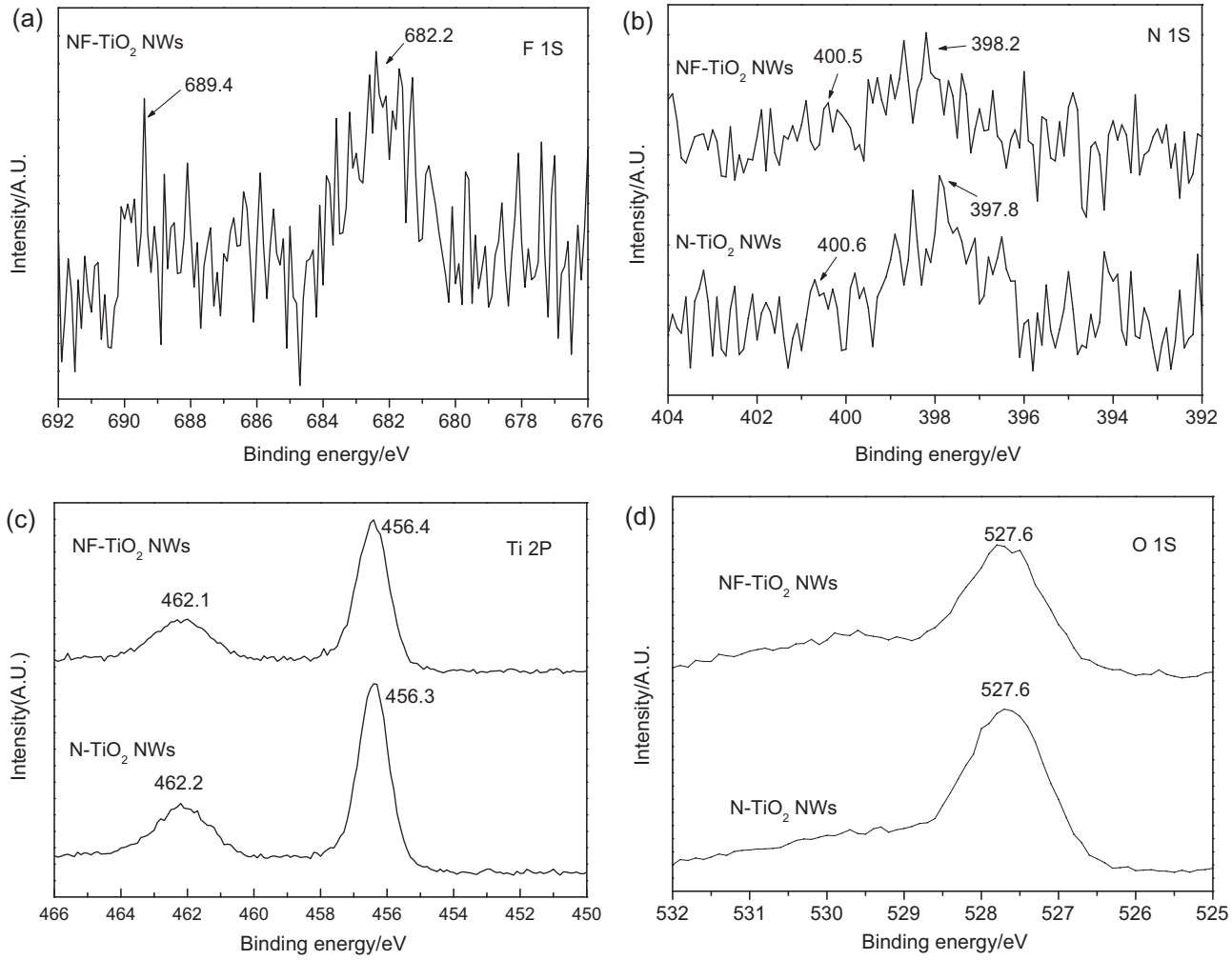

Fig. 4. XPS analysis of (a) F 1s, (b) N 1s, (c) Ti 2p and (d) O 1s for N–TiO_2 NWs and NF–TiO_2 NWs.

[41]. In this study, it was found that NF–TiO_2 nanorods instead of nanowires are formed when R_F is more than 0.35. The relatively less {0 0 1} crystal facet is produced (but more than 6%) because the value of R_F = 0.35 is low in the preparation of NF–TiO_2 NWs. Therefore, the percentage of {0 0 1} facet in this study is still very limited due to the limitation of R_F.

The synergistic functions of chemisorbed F to lower the surface energy and isopropanol to act as protective capping agent lead to the formation of TiO_2 NWs, which is a thermodynamically favored morphology under these conditions. Fluoride ions can markedly reduce the surface energy of the {0 0 1} surface to a level lower than that of {1 0 1} surface. This effect comes from the establishment of a new balance between O–O/F–O repulsions and Ti–O/Ti–F attractions, which stabilize Ti and O atoms on the surfaces [42]. The isopropanol plays multiple roles in this synthetic system for the formation of TiO_2 NWs. It acts not only as a reaction medium but also as a protecting agent to control the isotropic growth of TiO_2 single crystals because isopropanol tends to dissociate to form an alkoxy group ($(CH_3)_2CHO^-$) bound to coordinatively unsaturated Ti^{4+} cations on the crystal surfaces. The higher density of 5-fold Ti on crystal facet surfaces may lead to more selective adhesion of isopropanol, which restricts the growth of TiO_2 single crystals along [001] direction [39] to form nanowires.

Fig. 4 shows the XPS spectrum of atoms in the doped TiO_2 NWs prepared by the hydrothermal process. Fig. 4a shows the F 1s XPS spectra of the NF–TiO_2 NWs. The F 1s region is composed of two peaks. The peak located at 682.2 eV originated from the F-containing compounds (Ammonium fluoride) adsorbed on the surface of TiO_2 [43]. Another small peak at 689.4 eV could be attributed to the substitutional F atoms that occupied oxygen sites in the TiO_2 crystal lattice and form bond of Ti—F [44], meaning that F atoms were incorporated into the TiO_2 crystal lattice by the hydrothermal method. Based on XPS results, the content of F atoms are 0.34% for NF–TiO_2 NWs. Obviously, most of the F atoms in NF–TiO_2 NWs exist mainly in the form of F^- ions adsorbed on the surface of TiO_2 NWs, which can greatly reduce the surface energy of {0 0 1} facet. This result is in accordance with the analysis of HRTEM. On the contrary, only low amount of F atoms can be incorporated into the lattice of TiO_2.

Fig. 4b shows the XPS spectra for the N 1s region of N–TiO_2 and NF–TiO_2 NWs. A broad peak extending from 394 to 404 eV is observed for both N–TiO_2 NWs and NF–TiO_2 NWs, which is typical of nitrogen-doped titanium dioxide reported by other researchers [45]. In the spectra, a peak appeared at 399–400.0 eV was ascribed to the N atoms from N–N, N–H, and O–N [46]. A peak observed at 397–398 eV was generally considered as the evidence for the presence of Ti—N bonds formed when the N atoms replaced the oxygen in the TiO_2 crystal lattice [3]. It can be concluded that N atoms were incorporated into the TiO_2 crystal lattice by the hydrothermal process. The N content was 0.71% for N–TiO_2 NWs and 0.89% for NF–TiO_2 NWs. Livraghi et al. [47] also reported similar results that F^- ions substitute oxygen in the lattice of TiO_2 favoring N species incorporation in the TiO_2 and leading to higher N content than only N–TiO_2.

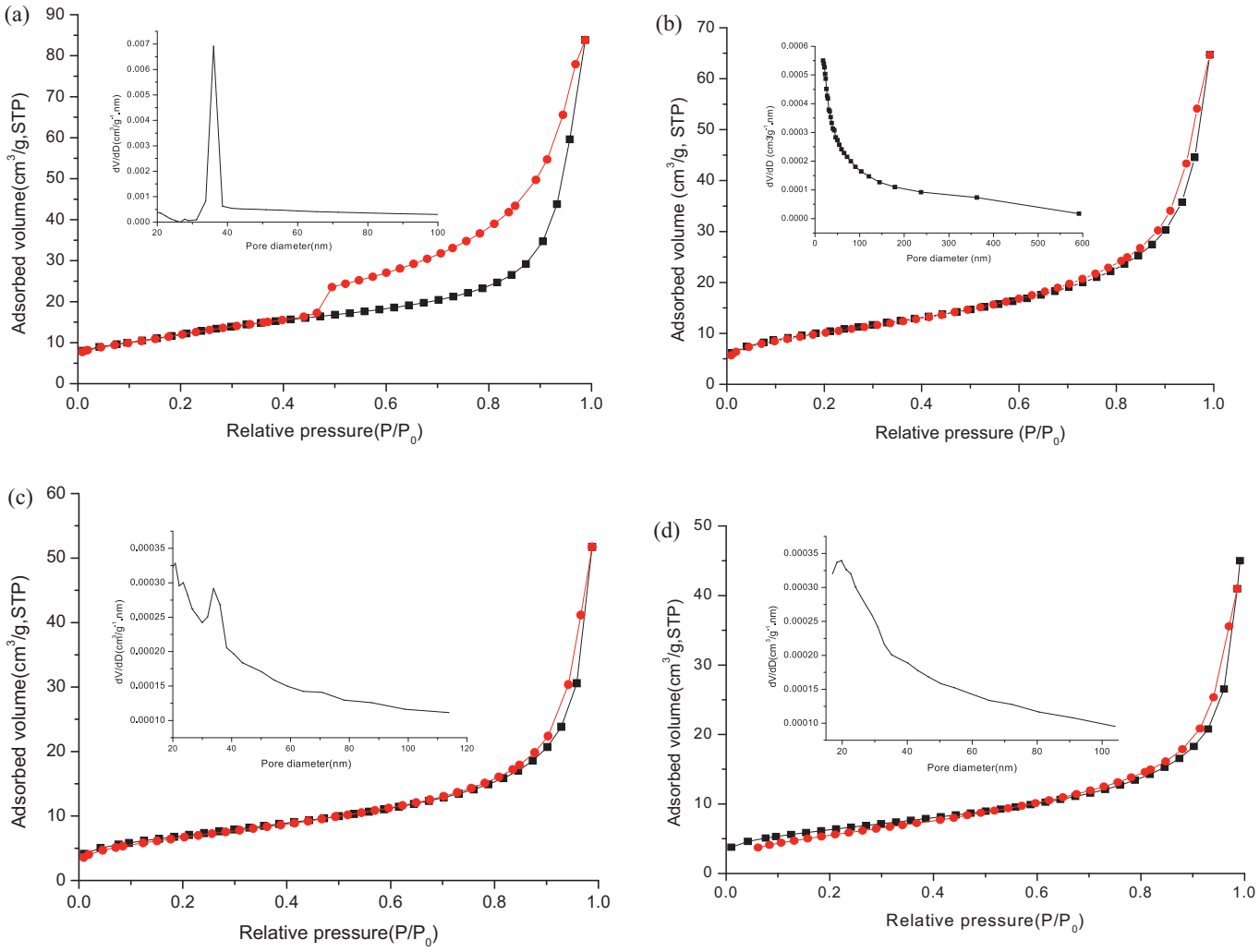

Fig. 5. N_2 adsorption and desorption isotherms and pore size distributions (insets) of (a) N–TiO_2 NPs, (b) NF–TiO_2 NPs, (c)N–TiO_2 NWs and (d) NF–TiO_2 NWs.

Fig. 4c and d shows the XPS spectra for the Ti 2p and O 1s region of N–TiO_2 NWs and NF–TiO_2 NWs, respectively. The Ti 2p region of two nanowires was similar and composed of two peaks. One peak at 456 eV (Ti $2p_{3/2}$) was attributed to the Ti^{4+} in doped TiO_2 NWs, while the other one at 462 eV (Ti $2p_{1/2}$) was assigned to the Ti^{3+} due to N or N,F doping converting some Ti^{4+} to Ti^{3+} by charge compensation. The O 1s region of two nanowires was also similar and composed of two peaks. One peak at 527.6 eV was attributed to the Ti–O in doped TiO_2, while the other one at 529.7 eV was assigned to the hydroxyl group. These XPS observation indicates that N or N,F-doping did not affect the structure of these non-metal doped TiO_2 NWs significantly.

The surface area and pore diameter distribution of N–TiO_2 nanoparticles (NPs), NF–TiO_2 NPs, N–TiO_2 NWs and NF–TiO_2 NWs calcined at 600 °C were investigated using nitrogen adsorption and desorption isotherms (shown in Fig. 5a, b, c, and d). The isotherms of these three samples are typical type IV-like with a type H_2 hysteresis loop, which indicates the formation of mesoporous materials according to IUPAC classification [48]. The plot of the pore size distribution (inset in Fig. 5a, b, c and d) was determined by using BJH method from the desorption branch of the isotherm. It shows that all samples clearly have mesoporous structure. The BET surface areas of N–TiO_2 NPs and NF–TiO_2 NPs were about 75.5 $m^2\,g^{-1}$ and 51.2 $m^2\,g^{-1}$, respectively. However, compared to N–TiO_2 NPs and NF–TiO_2 NPs, the area of the hysteresis loop of N–TiO_2 NWs and NF–TiO_2 NWs significantly decreased. The average pore diameter and the BET surface area of N–TiO_2 NWs and NF–TiO_2 NWs were about 3.5 nm and 2.2 nm, and 41.7 $m^2\,g^{-1}$ and 37.5 $m^2\,g^{-1}$, respectively. Even so, their surface areas are relatively larger than that of other hydrothermally synthesized nanowires [49]. These characteristics can also be confirmed by the TEM images observation, which presents some mesoporous structure (see Fig. 3a and c). The form of mesoporous structure may come from the escape of ammonia formed during urea decomposition in the process of hydrothermal synthesis.

Fig. 6 shows the UV–vis absorption spectra of N–TiO_2 NWs and NF–TiO_2 NWs calcined at 600 °C as well as the reference TiO_2 NWs. Effective bandgap was estimated from the Kubelka-Munk function F(R), where *R* is the absolute value of reflectance [50]. Among the doped and undoped TiO_2 NWs, NF–TiO_2 NWs exhibited the strongest absorption in the visible light range, where the reference TiO_2 NWs showed very low light absorption. The estimated effective bandgap for NF–TiO_2 NWs was 2.96 eV compared to 3.22 eV for the reference TiO_2 NWs, which is very close to that of the anatase TiO_2 phase (3.2 eV). In the case of the doped nanowires (N–TiO_2 NWs and NF–TiO_2 NWs), the adsorption edge was shifted to visible region, which indicates that nitrogen and fluorine were effectively incorporated into TiO_2 by the hydrothermal

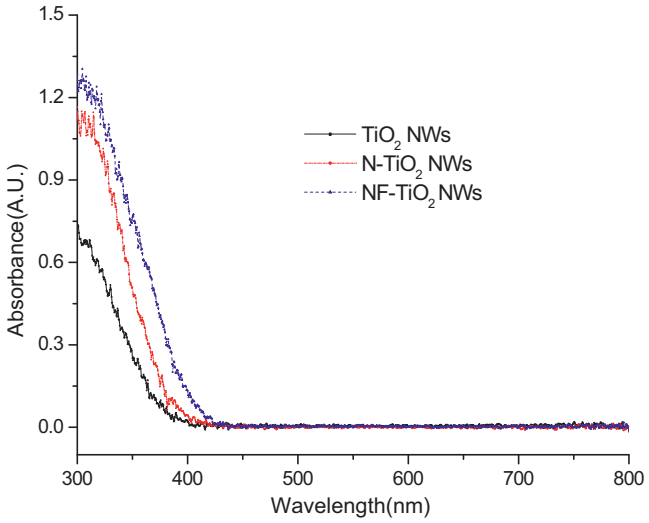

Fig. 6. UV–vis absorbance of doped and undoped TiO_2 NWs.

method to extend their photoresponse region toward the visible light.

The photocatalytic activity of N–TiO_2 NWs and NF–TiO_2 NWs was evaluated by decomposing atrazine in aqueous solution under visible light and UV irradiation. NF–TiO_2 NPs were used as a reference to compare with the photocatalytic activity of doped TiO_2 NWs under the same experimental condition. All doped photocatalysts effectively decomposed atrazine under visible light irradiation. NF–TiO_2 NWs presented the highest photocatalytic activity for the degradation of atrazine (>60% within 6 h). In order to confirm the photocatalytic activity of doped TiO_2 NWs under visible light irradiation, a control experiment was also performed. There was no remarkable concentration change of atrazine in 6 h under the visible light condition with the addition of TiO_2 NWs. These facts demonstrated that the degradation of atrazine mainly resulted from the effective doping with nitrogen, fluorine or both of them [51]. Usually the BET surface area plays an important role in adsorption and degradation. Compared with NF–TiO_2 NPs, the doped TiO_2 NWs have no advantages in the specific surface area and porosity even though their surface areas significantly increased in comparison with other prepared photocatalysts by hydrothermal method [52].

The experiments for the degradation of atrazine with doped nanoparticles and nanowires under UV irradiation were also performed (see Fig. 7b). Under UV irradiation without any photocatalysts, the concentration of atrazine decreased slightly, which may result from the photolysis of atrazine in the presence of UV [53]. The decrease in atrazine concentration in the presence of the N,F-doped TiO_2 NWs was more pronounced than that of N,F-doped TiO_2 NPs. This can be attributed to the higher charge carrier mobility and lower carrier recombination rate of nanowires than those of nanoparticles. The speed of electron diffusion across nanoparticle junctions is several orders of magnitude smaller than that of nanowire due to frequent electron trapping at the junctions of nanoparticles and separated charges are easily recombined before they reach the surface of nanoparticles [18].

It is notable that NF–TiO_2 NWs exhibited slightly higher photocatalytic activity than P25 powder for degradation of atrazine. Incredibly, the atrazine was completely degraded within 30 min. Moreover, it is also observed that the NF–TiO_2 NWs exhibited far higher photocatalytic activity than N–TiO_2 NWs for degradation of atrazine.

A possible explanation is that N,F-doped TiO_2 NWs possess a strong photocatalytic effect. It is generally accepted that surface

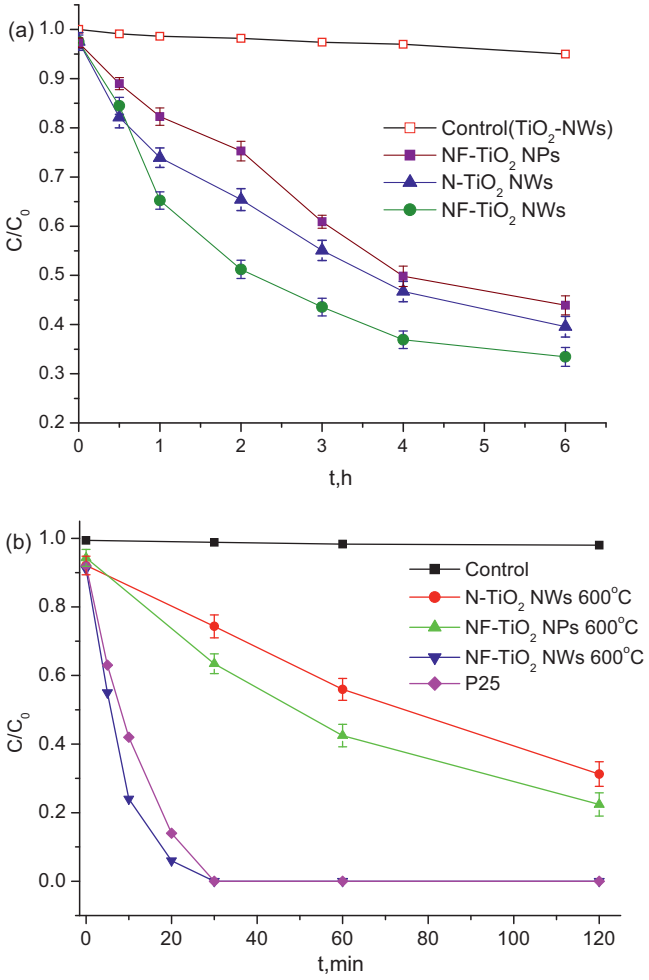

Fig. 7. Photocatalytic degradation of atrazine irritated by (a) visible light and (b) UV (The error bars are referred to the range of C/C_0 value when three separate experiments of photocatalytic degradation were performed).

atomic structure inherently determines the reactivity of heterogeneous catalysts. Often, facets with a higher percentage of undercoordinated atoms are reactive. Indeed, Fig. 3d displays the more percentage of {0 0 1} facet, indicating that enhanced energy harvesting may contribute to the strong photocatalytic activity. Murakami et al. [54] reported that TiO_2 particles with specific exposed crystal facets showed higher photocatalytic activity than commercial P25, suggesting that the recombination of photogenerated electrons and holes was inhibited by spatial separation of redox sites due to selective migration of negative electrons and positive holes to specific exposed crystal faces and/or different reactivity of electrons and holes on the specific exposed crystal face. Similar results were reported by Ohno et al. [55] and Xiang et al. [56]. The photocatalytic activity toward degradation of pollutants on anatase TiO_2 with more exposed {0 0 1} facet is higher than that of TiO_2 with more exposed {1 0 1} facet.

Generally, heat treatment promotes the crystallinity of anatase, but the transformation of anatase to rutile in undoped titanium usually occurs around 600 °C [36]. Due to its poor photocatalytic activity, the approach of extending the anatase to rutile transformation temperature above 600 °C to promote the crystallinity of anatase is worthy to develop. In this study, as one of coexistence of the solid phase in this TiO_2 NWs shown in Fig. 1, the TiO_2 (B) is still present at 700 °C, the retention of the anatase phase up to 700 °C can be attributed to the presence of TiO_2 (B). From these observations it can be concluded that improving the crystallinity by extending

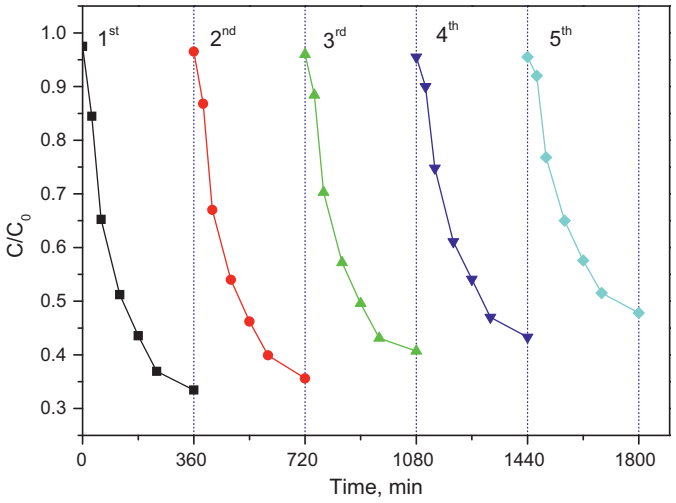

Fig. 8. Photocatalytic activities of N,F–TiO_2 NWs for atrazine degradation with 5 times uses.

the anatase-to-rutile transformation temperature enables us to achieve enhanced photocatalytic activity.

In addition, according to the results of XPS, there are substitutional F and N atoms in NF–TiO_2 NWs. We ascribe the different absorption band position in NF–TiO_2 NWs to the synergistic effect of N and F doping, which results in the enhanced photocatalytic activity. We infer that the energy level position of electron or hole produced by visible light absorption in the N/F substituted TiO_2 is more conducive to the generation of reactive groups than that of single N doped TiO_2.

It is found that NF–TiO_2 NWs can be easily separated from the aqueous suspension containing the nanowire photocatalyst simply by sedimentation. The photocatalytic activity of separated photocatalyst was subsequently evaluated by a series of recycling and reuse tests. The results shown in Fig. 8 indicate that there is no significant decrease in the photocatalytic activity over the test period, which implies that the synthesized nanowires have the promising potential in industrial application.

4. Conclusions

A facile hydrothermal method has been developed to prepare NF–TiO_2 NWs using titanium sulfate as a precursor. The method does not require complicated procedures, template support and high-temperatures in the flow of nitrogen or ammonia gas. Photocatalytic activity measurements show that the N,F-codoped TiO_2 NWs calcined at 600 °C presents the highest photocatalytic performance for the degradation of atrazine under UV or visible light irradiation compared to N,F-codoped TiO_2 NPs and N-doped TiO_2 NWs. These benefits come from the synergistic effect of N and F doping, inhibiting the transformation of anatase to rutile as well as the relatively more reactive {0 0 1} crystal facet in addition to the advantages of 1D structure nanomaterials.

Acknowledgement

This work was partially funded by the Cyprus Research Promotion Foundation through Desmi 2009–2010 which is co-funded by the Republic of Cyprus and the European Regional Development Fund of the EU under contract number NEA IPODOMI/STRATH/0308/09.

Changseok Han acknowledged the Graduate School Dean's Fellowship, which supports University of Cincinnati doctoral students in their final year of degree work.

References

[1] P.M. Ajayan, S. Iijima, Nature 361 (6410) (1993) 333–334.
[2] M. Grätzel, Nature 414 (2001) 338–344.
[3] K. Pathakoti, S. Morrow, C. Han, M. Pelaez, X. He, D.D. Dionysiou, H. Hwang, Environ. Sci. Technol. 47 (2013) 9988–9996.
[4] Q. Lu, Z. Lu, Y. Lu, L. Lv, Y. Ning, H. Yu, Y. Hou, Y. Yin, Nano Lett. 13 (2013) 5698–5702.
[5] Y. Wu, M. Xing, B. Tian, J. Zhang, F. Chen, Chem. Eng. J. 162 (2010) 710–717.
[6] C. Han, J. Andersen, V. Likodimos, P. Falaras, J. Linkugel, D.D. Dionysiou, Catal. Today 224 (2014) 132–139.
[7] K. Kondo, N. Murakami, C. Ye, T. Tsubota, T. Ohno, Appl. Catal. B: Environ. 142–143 (2013) 362–367.
[8] W. Zhao, W. Ma, C. Chen, J. Zhao, Z. Shuai, J. Am. Chem. Soc. 126 (2004) 4782–4783.
[9] J.C. Yu, J.G. Yu, W.K. Ho, Z.T. Jiang, L.Z. Zhang, Chem. Mater. 14 (2002) 3808–3816.
[10] Y. Komai, K. Okitsu, R. Nishimura, N. Ohtsu, G. Miyamoto, T. Furuhara, S. Semboshi, Y. Mizukoshi, N. Masahashi, Catal.Today 164 (2011) 399–403.
[11] W. Jiao, N. Li, L. Wang, L. Wen, F. Li, G. Liu, H. Cheng, Chem. Commun. 49 (2013) 3461–3463.
[12] D. Chen, Z. Jiang, J. Geng, Q. Wang, D. Yang, Ind. Eng. Chem. Res. 46 (2007) 2741–2746.
[13] G. Dai, S. Liu, Y. Liang, H. Liu, Z. Zhong, J. Mol. Catal. A: Chem. 368–369 (2013) 38–42.
[14] P. Wang, T. Zhou, R. Wang, T. Lim, Water Res. 45 (2011) 5015–5026.
[15] S. In, A. Orlov, R. Berg, F. Garcua, S.P. Jimenez, M.S. Tikhov, D.S. Wright, R.M. Lambert, J. Am. Chem. Soc. 129 (2007) 13790–13791.
[16] V. Gombac, L. De Rogatis, A. Gasparotto, G. Vicario, T. Montini, D. Barreca, G. Balducci, P. Fornasiero, E. Tondello, M. Graziani, Chem. Phys. 339 (2007) 111–123.
[17] H. Yin, G. Ding, B. Gao, F. Huang, X. Xie, M. Jiang, Mater. Res. Bull. 47 (2012) 3124–3128.
[18] A.C. Fisher, L.M. Peter, E.A. Ponomarev, A.B. Walker, K.G.U. Wijayantha, J. Phys Chem. B 104 (2000) 949–958.
[19] M. Paulose, K. Shankar, O.K. Varghese, G.K. Mor, B. Hardin, C.A. Grimes, Nanotechnology 17 (2006) 1446.
[20] K. Shankar, G.K. Mor, H.E. Prakasam, S. Yoriya, M. Paulose, O.K. Varghese, C.A. Grimes, Nanotechnology 18 (2007) 65707.
[21] M.A. Khan, H.T. Jung, O.B. Yang, J. Phys. Chem. B 110 (2006) 6626–6630.
[22] X. Zhang, J. Pan, A. Du, W. Fu, D.D. Sun, J.O. Leckie, Water Res. 43 (2009) 1179–1186.
[23] H. Wang, Y. Liu, H. Huang, M. Zhong, H. Shen, Appl. Phys. A 97 (2009) 25–29.
[24] Y. Wang, H. Yang, H. Xu, Mater. Lett. 64 (2010) 164–166.
[25] R. Yoshida, Y. Suzuki, S. Yoshikawa, J. Solid State Chem. 178 (2005) 2179–2185.
[26] S. Yoshikazu, Y. Susumu, J. Mater. Res. 19 (2004) 982–985.
[27] A.R. Armstrong, G. Armstrong, J. Canales, R. Garaca, P.G. Bruce, Adv. Mater. 17 (2005) 862–865.
[28] P.G. Wu, C.H. Ma, J.K. Shang, Appl. Phys. A 81 (2005) 1411–1417.
[29] M. Masahiko, W. Teruyoshi, J. Electrochem. Soc. 153 (2006) 186–190.
[30] X. Peng, A. Chen, J. Mater. Chem. 14 (2004) 2542–2548.
[31] K. Huo, X. Zhang, L. Hu, X. Sun, J. Fu, P.K. Chu, Appl. Phys. Lett. 93 (2008) 013105-1–013105-3.
[32] B. Liu, J.E. Boercker, E.S. Aydi, Nanotechnology 19 (2008) 505604.
[33] A. Yu, G. Wu, F. Zhang, Y. Yang, N. Guan, Catal. Lett. 129 (2009) 507–512.
[34] C. Han, V. Likodimos, J.A. Khan, M.N. Nadagouda, J. Andersen, P. Falaras, P. Rosales-Lombardi, D.D. Dionysiou, Environ. Sci. Pollut. Res. 21 (2014) 11781.
[35] X. Zhang, A.J. Dua, P. Lee, D.D. Sun, J.O. Leckie, J. Membrane Sci. 313 (2008) 44–51.
[36] W. Li, Y. Bai, C. Liu, Z. Yang, X. Feng, X. Lu, N.V.D. Laak, K. Chan, Environ. Sci. Technol. 43 (2009) 5423–5428.
[37] H.B. Jiang, Q. Cuan, C.Z. Wen, J. Xing, D. Wu, X.Q. Gong, C. Li, H.G. Yang, Angew. Chem. Int. Ed. 50 (2011) 3764–3768.
[38] H.G. Yang, C.H. Sun, S.Z. Qiao, J. Zou, G. Liu, S.C. Smith, H.M. Cheng, G.Q. Lu, Nature 453 (2008) 638–641.
[39] H. Yang, G. Liu, S.Z. Qiao, C.H. Sun, Y.G. Jin, S.C. Smith, J. Zou, H.M. Cheng, G.Q. Lu, J. Am. Chem. Soc. 131 (2009) 4078–4083.
[40] D. Zhang, G. Li, X. Yang, J.C. Yu, Chem. Commun. (2009) 4381–4383.
[41] J.G. Yu, Q.J. Xiang, J.R. Ran, S. Mann, CrystEngComm 12 (2010) 872–879.
[42] C.K. Nguyen, H.G. Cha, Y.S. Kang, Cryst. Growth Des. 11 (2011) 3947–3953.
[43] J.C. Yu, J.G. Yu, W.K. Ho, Z.T. Jiang, L.Z. Zhang, Chem. Mater. 14 (2002) 3808–3816.
[44] D. Li, H. Haneda, S. Hishita, N. Ohashi, Chem Mater. 17 (2005) 2596–2602.
[45] S. Sakthivel, M. Janczarek, H. Kisch, J. Phys. Chem. B 108 (2004) 19,384–19387.
[46] T. Morikawa, R. Asahi, T. Ohwaki, K. Aoki, Y. Taga, Jpn. J. Appl. Phys. 40 (2001) 561–563.
[47] S. Livraghi, K. Elghniji, A.M. Czoska, M.C. Paganini, E. Giamello, M. Ksibi, J. Photochem. Photobiol. A 205 (2009) 93–97.
[48] S.J. Gregg, K.S.W. Sing, Adsorption, Surface Area Porosity, Academic Press, London, 1997, pp. p.111.
[49] A. Hu, X. Zhang, K.D. Oakes, P. Peng, Y.N. Zhou, M.R. Servos, J. Hazard. Mater. 189 (2011) 278–285.
[50] T. Toyoda, H. Kawano, Q. Shen, A. Kotera1, M. Ohmori, Jpn. J. Appl. Phys. 39 (2000) 3160–3163.

[51] S. Livraghia, K. Elghnijib, A.M. Czoskaa, M.C. Paganinia, E. Giamelloa, M. Ksibib, J. Photochem. Photobiol. 205 (2009) 93–97.
[52] A. Hu, X. Zhang, K.D. Oakes, P. Peng, Y.N. Zhou, M.R. Servos, J. Hazard. Mater. 189 (2011) 278–285.
[53] S. Jaina, R. Yamgarb, R.V. Jayaram, Chem. Eng. J. 148 (2009) 342–347.
[54] N. Murakami, Y. Kurihara, T. Tsubota, T. Ohno, J. Phys. Chem. C 113 (2009) 3062–3069.
[55] T. Ohno, K. Sarukawa, M. Matsumura, New J. Chem. 26 (2002) 1167–1170.
[56] Q.J. Xiang, K.L. Lv, J.G. Yu, Appl. Catal. B: Environ. 96 (2010) 557–564.